Journal of Coordination Chemistry

ISSN: (Print) (Online) Journal homepage: https://www.tandfonline.com/loi/gcoo20

Biomass-derived *rctt*-3,4-di-2-furanyl-1,2-cyclobutanedicarboxylic acid: a polytopic ligand for synthesizing green metal-organic materials

Rahul K. Shahni, Houssein Amjaour, Briana Krupinsky, Sarah Reagen, Zijun D. Wang, Xu Wu, Dominic Nkemngong, Julia X. Zhao, Angel Ugrinov, Joseph Robertson & Qianli Rick Chu

To cite this article: Rahul K. Shahni, Houssein Amjaour, Briana Krupinsky, Sarah Reagen, Zijun D. Wang, Xu Wu, Dominic Nkemngong, Julia X. Zhao, Angel Ugrinov, Joseph Robertson & Qianli Rick Chu (2021) Biomass-derived *rctt*-3,4-di-2-furanyl-1,2-cyclobutanedicarboxylic acid: a polytopic ligand for synthesizing green metal-organic materials, Journal of Coordination Chemistry, 74:1-3, 226-240, DOI: 10.1080/00958972.2021.1878500

To link to this article: https://doi.org/10.1080/00958972.2021.1878500

JOURNAL OF COORDINATION CHEMISTRY
2021, VOL. 74, NOS. 1–3, 226–240
https://doi.org/10.1080/00958972.2021.1878500

Biomass-derived *rctt*-3,4-di-2-furanyl-1,2-cyclobutanedicarboxylic acid: a polytopic ligand for synthesizing green metal-organic materials

Rahul K. Shahni[a], Houssein Amjaour[a], Briana Krupinsky[a], Sarah Reagen[a], Zijun D. Wang[a], Xu Wu[a], Dominic Nkemngong[a], Julia X. Zhao[a], Angel Ugrinov[b], Joseph Robertson[a] and Qianli Rick Chu[a]

[a]Department of Chemistry, University of North Dakota, Grand Forks, ND, USA; [b]Department of Chemistry and Biochemistry, North Dakota State University, Fargo, ND, USA

ABSTRACT

Biomass is an abundant and environmentally friendly source for materials that can be used in a multitude of applications in the effort to replace petrochemicals. Furfural and malonic acid are biomass-sourced platforms that can be utilized in the synthesis of biobased compounds; *rctt*-3,4-di-2-furanyl-1,2-cyclobutanedicarboxylic acid (CBDA-2) is one such compound. In this study, CBDA-2 has been introduced into metal-organic materials chemistry as a semi-rigid polytopic ligand. This compound has been utilized as a polytopic ligand in the formation of two different 2D coordination polymers with Cu^{2+} and Co^{2+} as the metal centers via a conventional solution method. Both complexes have been characterized by X-ray crystal structure determination and showed visual thermochromic behaviors. This study demonstrates that CBDA-2 is a promising green building block in coordination chemistry.

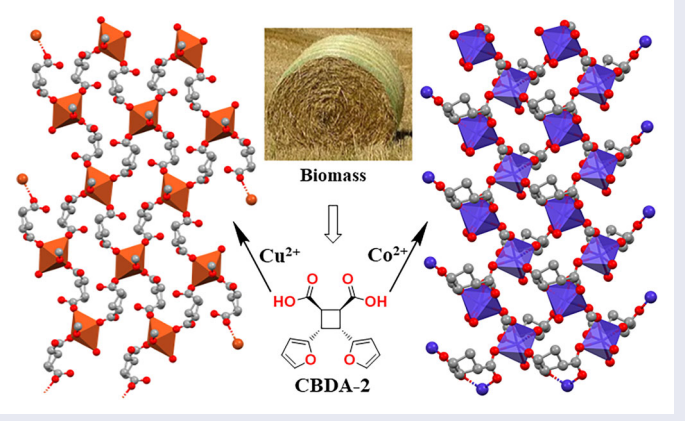

ARTICLE HISTORY
Received 14 December 2020
Accepted 10 January 2021

KEYWORDS
Furfural; bioadvantaged chemical; cyclobutane; diacid; chelating ligand

CONTACT Qianli Rick Chu chu@chem.und.edu Department of Chemistry, University of North Dakota, Grand Forks, ND, USA

Supplemental data for this article is available online at https://doi.org/10.1080/00958972.2021.1878500.

1. Introduction

Increasing awareness of environmental protection and continuous shrinking of the earth's finite fossil resources has inspired extensive study into the use of biomass-derived compounds to replace fossil feedstocks in the manufacture of a variety of products [1, 2]. Petrochemicals are still the major starting materials for synthesizing all kinds of ligands used in coordination chemistry. However, the inherent composition of carbon, hydrogen, and oxygen in biomass leads to its suitability as a starting material for the synthesis of oxygen-rich ligands (Figure 1). As important members of the polytopic ligand family, oxygen-rich ligands [3–6], including many carboxylates are crucial in constructing metal-organic materials with different applications such as catalysis, gas separation, and detection of volatile organic compounds [7–10]. To the best of our knowledge, there is still no polytopic ligand specifically designed and synthesized from biomass-derived chemicals [11, 12].

In this study, we reported a polytopic ligand, *rctt*-3,4-di-2-furanyl-1,2-cyclobutanedicarboxylic acid (CBDA-2, Scheme 1), synthesized from two bioadvantaged chemicals (*i.e.,* furfural and malonic acid) [13–15]. Furfural is an important renewable feedstock, which is mainly produced from hemicellulose of crop residues such as corncobs, sugarcane bagasse, and wheat bran [16, 17]. Bio-production of malonic acid involves the use of genetically modified yeast cells to ferment sugar directly into malonic acid with up to over 100% yield due to carbon dioxide sequestration during the process [18, 19]. The polytopic ligand, CBDA-2, yielded from biomass has the potential to become a useful green building block, which will make metal-organic materials more environmentally friendly. To demonstrate the potential application of this multifunctional ligand, two different two-dimensional (2D) coordination polymers have been synthesized via a conventional solution method using copper and cobalt salts, respectively. We hope that our study will initiate more work into the design, synthesis, and application of biomass-derived ligands to make coordination chemistry more sustainable.

2. Experimental

2.1. Chemicals and measurements

All chemicals were purchased from Alfa Aesar, Sigma-Aldrich, or Acros, and used without purification. Blacklight used in the photoreaction was 15 W Eiko EK15526 F15T8/BL. The solution phase nuclear magnetic resonance spectra (NMR) were recorded with

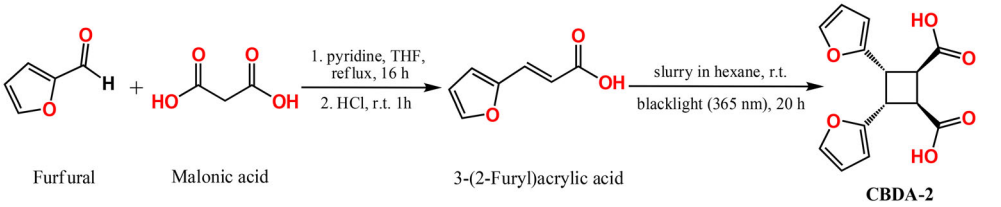

Scheme 1. Synthesis of a polytopic ligand, CBDA-2, from two bioadvantaged chemicals: furfural and malonic acid.

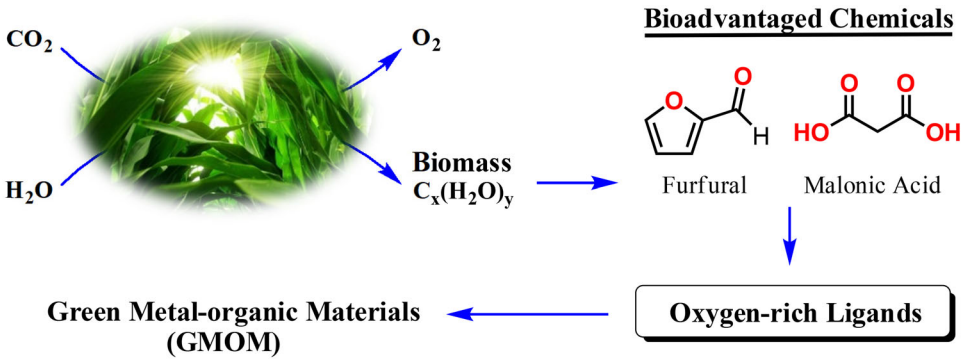

Figure 1. Synthesis of green metal-organic materials (GMOM) from biomass via bioadvantaged chemicals and oxygen-rich ligands.

a Bruker AVANCE (^{1}H: 500 MHz, ^{13}C: 125 MHz). Proton and carbon chemical shifts were reported in ppm downfield from tetramethylsilane (TMS) or using the resonance of corresponding deuterated solvent as an internal standard. Single-crystal X-ray data were collected on a Bruker Kappa Apex II Duo X-Ray Diffractometer with Cu $K\alpha$ ($\lambda = 1.54178$ Å) radiation. Fourier-transform infrared spectra (FT-IR) were recorded on a Thermo Scientific Nicolet iS5 FT-IR spectrometer. Differential scanning calorimetry (DSC) was recorded with Perkin Elmer Jade DSC with a ramping rate of 20 °C/min under nitrogen. Heat flow was recorded from both the first heating and cooling curve. Thermogravimetric analysis (TGA) was carried out with a Hi-Res TGA Q500 from TA Instruments using alumina pans at a heating rate of 20 °C/min under nitrogen with a sample weight of 10 mg.

2.2. Synthesis of rctt-3,4-di(furan-2-yl)cyclobutane-1,2-dicarboxylic acid (CBDA-2)

The synthetic procedure of CBDA-2 reported herein is developed by improving our previous approach (Scheme 1) [14]. This procedure is scalable and operator friendly. Specifically, CBDA-2 was synthesized by photodimerization of 2-furanacrylic acid (FAA) in a slurry using hexane as a reaction medium. The typical process involves suspending 5.0 g of crystalline FAA in hexane in a 250 mL Erlenmeyer flask with magnetic stirring. The vigorously stirred suspension was kept between six 15-watt Eiko blacklights for 12 h. The powder clustered on the inside wall of the flask was loosened using a spatula or sonication when necessary during the reaction. The slurry was then filtered and CBDA-2 was obtained as a white solid in 91% yield (4.5 g, m.p. 170–171 °C). ^{1}H NMR (DMSO-d_6, 500 MHz) δ 12.52 (s, 2H), 7.43 (d, J = 2.5 Hz 2H), 6.28 (dd, 2H), 6.11 (d, J = 3.5 Hz 2H), 4.03(m, 2H), 3.68 (m, 2H); ^{13}C NMR (DMSO-d_6, 125 MHz) δ 38.3, 43.0, 107.9, 110.4, 142.6, 153.1, 173.6; IR (solid-state using ATR detector, ν, cm^{-1}) 2959 (m, C–H bending), 1696 (s, C = O stretching), 1503, 1415, 1349 (s, C = C aromatic), 1257 (m, C–O stretching), 1011 (m, out-of-plane OH).

Table 1. Crystal data of CBDA-2, CBDA-2·Et_3N, 1 and 2.

Crystal	CBDA-2[a]	CBDA-2·Et_3N	Cu-CBDA-2 Complex (**1**)	Co-CBDA-2 Complex (**2**)
CCDC #	1578122	2049902	2049903	2049905
Formula	$C_{14}H_{12}O_6$	$C_{20}H_{27}NO_6$	$C_{30}H_{30}CuO_{14}$	$C_{30}H_{32}Co_2O_{16}$
FW	276.24	377.42	678.08	766.41
Crystal size (mm)	0.34 × 0.08 × 0.04	0.39 × 0.23 × 0.20	0.20 × 0.15 × 0.04	0.19 × 0.14 × 0.04
Crystal system	Monoclinic	Triclinic	Orthorhombic	Orthorhombic
Space group	P 2_1/c	P-1	Pbca	Pna2_1
a (Å)	15.8528(7)	9.1495(3)	7.5903(3)	6.9274(3)
b (Å)	5.4219(3)	9.9671(4)	14.4036(7)	33.4102(12)
c (Å)	15.2918(7)	11.0579(4)	26.3037(11)	6.8234(3)
α (°)	90	82.6770(10)	90	90
β (°)	113.218	76.9120(10)	90	90
γ (°)	90	75.4290(10)	90	90
V (Å^3)	1207.92	947.97(6)	2875.72	1579.25
Temp. (K)	100(2)	100(2)	106(2)	105(2)
ρcalc (g·cm^{-3})	1.519	1.322	1.566	1.612
μ (mm^{-1})	1.023	0.804	1.736	8.913
Radiation type	CuK\a	CuK\a	CuK\a	CuK\a
F(000)	576	404	1404	788.0
No. of measured refl.	7726	12048	14792	7413
No. of independent refl.	2099	3264	2541	2368
No. of refl. (I ≥ 2σ)	1851	3086	2022	2152
R1/wR2 (I ≥ 2σ) (%)	11.60/4.14	10.20/3.86	15.93/6.82	9.68/4.24
R1/wR2 (all data) (%)	12.13/4.69	10.36/4.03	16.52/8.36	9.86/4.75

[a]Taken from our recent publication for comparison [14].

2.3. Synthesis of CBDA-2·Et_3N

CBDA-2 (0.275 g, 0.1 mmol) was dissolved in 5 mL methanol. Triethylamine (28 uL, 0.2 mmol, 2 equiv.) was first diluted with 3 mL methanol, and then added into the CBDA-2 solution dropwise with magnetic stirring. After filtration, the solution was kept in a 15 mL vial with a porous lid. Colorless crystals formed in two weeks (Table 1). It is remarkable that only one of the two carboxylic acids was deprotonated although two equivalents of triethylamine were used (See ESI for images).

2.4. Synthesis of Cu-CBDA-2 (1)

CBDA-2 (0.55 g, 0.2 mmol) was dissolved in 10 mL of methanol and to this a solution of $Cu(NO_3)_2{\cdot}3H_2O$ (0.24 g, 0.1 mmol) in 10 mL of deionized water was added dropwise. Then this reaction mixture was allowed to stir for 30 min. After that, a 1 M NaOH solution was added dropwise to the reaction mixture until a slight amount of precipitate began to form. The precipitate was then filtered off, and the filtrate was kept at room temperature [20]. After several days, turquoise crystals were produced (Table 1). The crystals were washed with water and methanol, respectively, and then dried in vacuum overnight. The yield of **1** crystals was 52% based on the metal salt. FT-IR (υ, cm^{-1}): 1698 (br, C = O from carboxylic acid), 2943 (m, C–H), 1549 (s, C = O asymmetric for carboxylate ion), 1612 (s, C = C aromatic), 1418 (m, C = O symmetric), 1276 (m, C–O), 1013 (w), 727 (s), 596 (m).

2.5. Synthesis of Co-CBDA-2 (2)

A similar process was used as in the case of **1**, but $Co(NO_3)_2{\cdot}6H_2O$ (0.29 g, 0.1 mmol) was used with an equimolar amount of CBDA-2 (0.27 g, 0.1 mmol). After a few days,

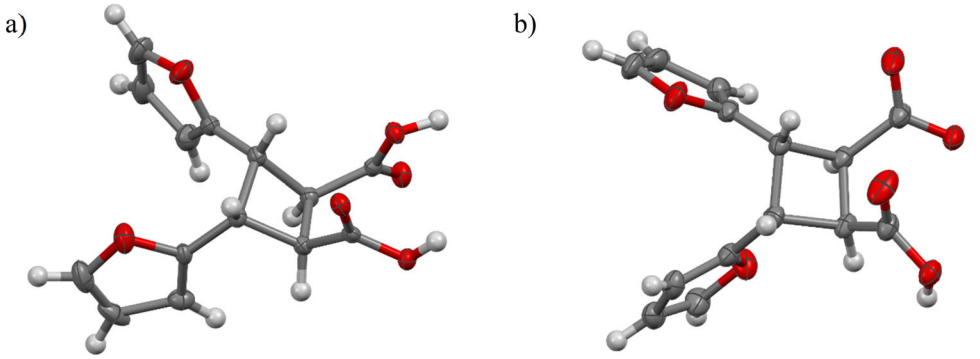

Figure 2. Crystal structures of (a) CBDA-2 and (b) CBDA-2 anion (a disordered Et_3NH^+ is omitted for clarity) in Oak Ridge Thermal Ellipsoid Plot (ORTEP) at the 50% probability level except for the hydrogen atoms.

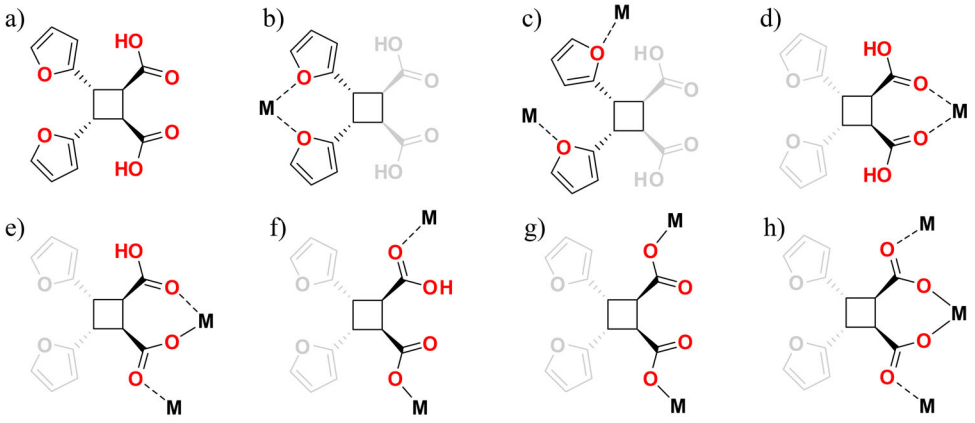

Figure 3. Chemical structure of CBDA-2 (shown in black and red), and seven coordination modes that furan rings and carboxylic acid/carboxylates of CBDA-2 may adopt to interact with metals or metal cations (shown in black, red, and gray).

light pink colored crystals of **2** were obtained (Table 1). The yield was 61% based on the metal salt. FT-IR (υ, cm^{-1}): 3316 (br, O–H), 1564 (s, C = O asymmetric), 1435 (m, C = O symmetric), 1019 (w), 722 (s).

3. Results and discussion

3.1. Description of CBDA-2 structure

The crystal structure of CBDA-2 is provided in Figure 2(a), while Figure 2(b) displays a CBDA-2 anion with one of the two carboxylic acids deprotonated. The disordered counter ion, triethylammonium, is omitted in Figure 2(b) for clarity (see ESI for the crystal structure with the triethylammonium). Both crystal structures are shown in Oak Ridge Thermal Ellipsoid Plot (ORTEP) at the 50% probability level except for the hydrogen atoms. While the two furan rings in Figure 2(a) are roughly pointing towards the same direction, they are oriented towards the opposite directions in Figure 2(b),

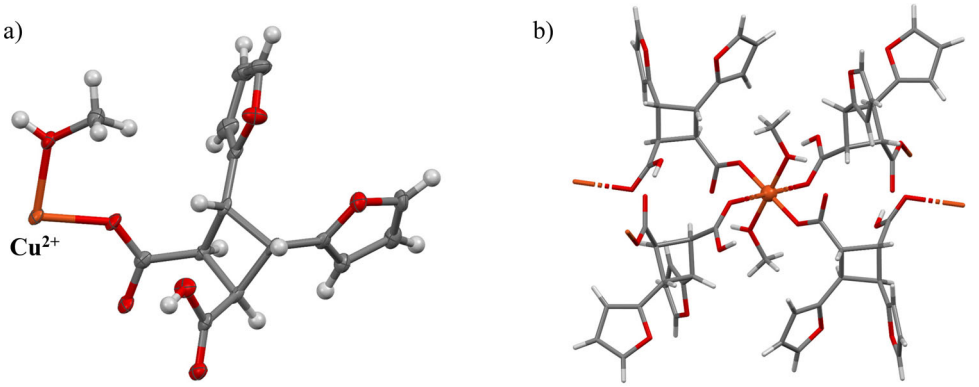

Figure 4. (a) Asymmetric unit of Cu-CBDA-2 (**1**) in Oak Ridge Thermal Ellipsoid Plot (ORTEP) at the 50% probability level except for the hydrogen atoms; (b) Octahedral Cu^{2+} center with four CBDA-2 molecules and two MeOH molecules.

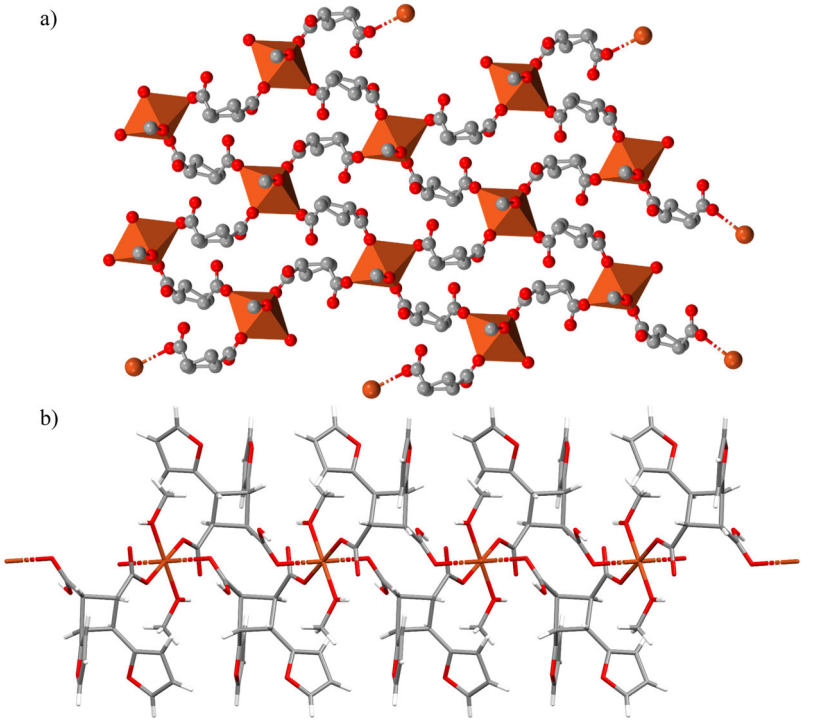

Figure 5. (a) Top view of Cu-CBDA-2 (**1**) shown in polyhedral style (the furan substituents are omitted for clarity.); (b) Side view of the 2D complex (**1**) along crystallographic *a* axis shown in Capped Sticks style.

confirming the furan rings can rotate around the carbon-carbon single bond between the five- and four-membered rings.

As shown in Figure 3(a), each CBDA-2 molecule contains two carboxylic acids and two furan rings, which can interact with metals or metal cations to form complexes. Figure 3(b) and 3(c) displays that the two sp^2 hybridized oxygens in its furan rings

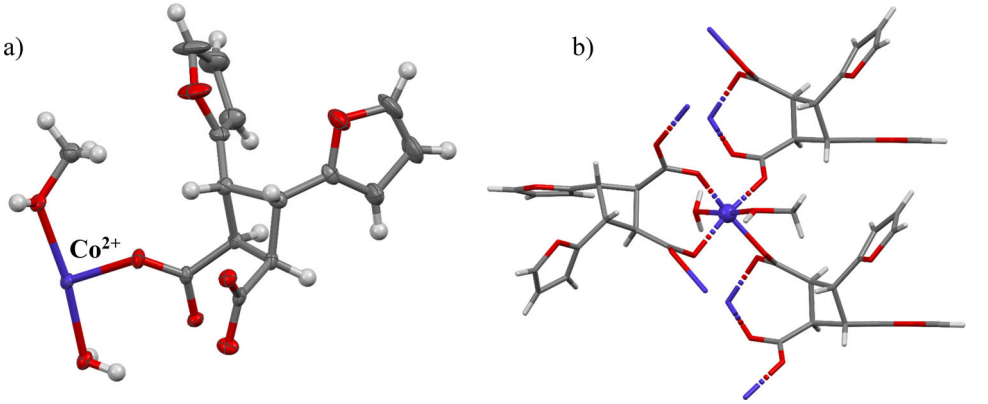

Figure 6. (a) Asymmetric unit of Co-CBDA-2 (**2**) in ORTEP at the 50% probability level except for the hydrogen atoms; (b) Octahedral Co^{2+} center interacting with three CBDA-2 molecules, one MeOH, and one H_2O molecule.

may interact with metal collaboratively or individually [21–23]. Figure 3(d)–3(h) exhibits five different ways that the two carboxylic acids or the corresponding carboxylate ion may interact with metal or metal cation [24–26]. Although the furan rings and carboxylic acids within the same CBDA-2 molecule may interact with different metal atoms or cations simultaneously, it is unlikely that they will interact with the same metal/metal cation since they are bonded to the same cyclobutane ring and trans to each other. It is worth mentioning that, besides what are shown in Figure 3, there are other possible ways that CBDA-2 may interact with metals or metal cations. For example, the electron-rich furan ring may interact with a metal cation via its π electrons [27].

Meanwhile, the cyclobutane core/linker of CBDA-2 has two exchangeable conformations (i.e. puckered vs. planar) with approximately 23° difference between them [14, 28–31]. The semi-rigid nature of cyclobutane will offer CBDA-2 a unique and useful balance between typical flexible aliphatic or rigid aromatic linkers in forming metal-organic materials.

3.2. Structure description of Cu-CBDA-2 (1)

Figure 4(a) presents the asymmetric unit of Cu-CBDA-2 (**1**) in Oak Ridge Thermal Ellipsoid Plot (ORTEP). The ratio of Cu:CBDA-2:MeOH in **1** is 1:2:2. As shown in Figure 4(b), the Cu^{2+} adopts an octahedral geometry with four CBDA-2 molecules interacting with the metal cation in the equatorial basal plane and two methanol molecules at the axial positions. Two of the four CBDA-2 molecules are deprotonated, which balance the charges on the Cu cation. The two deprotonated carboxylate oxygens are located on opposite sides of the Cu^{2+} center with the O^{-}-Cu^{2+}-O^{-} angle 180.0° and O^{-}-Cu^{2+} bond distance 1.923 Å. The two carbonyl groups in the non-deprotonated acids and two oxygen atoms in the two MeOH molecules are also located at the exact opposite direction of the Cu^{2+} center, with O-Cu^{2+} distances 2.446 and 1.984 Å, respectively.

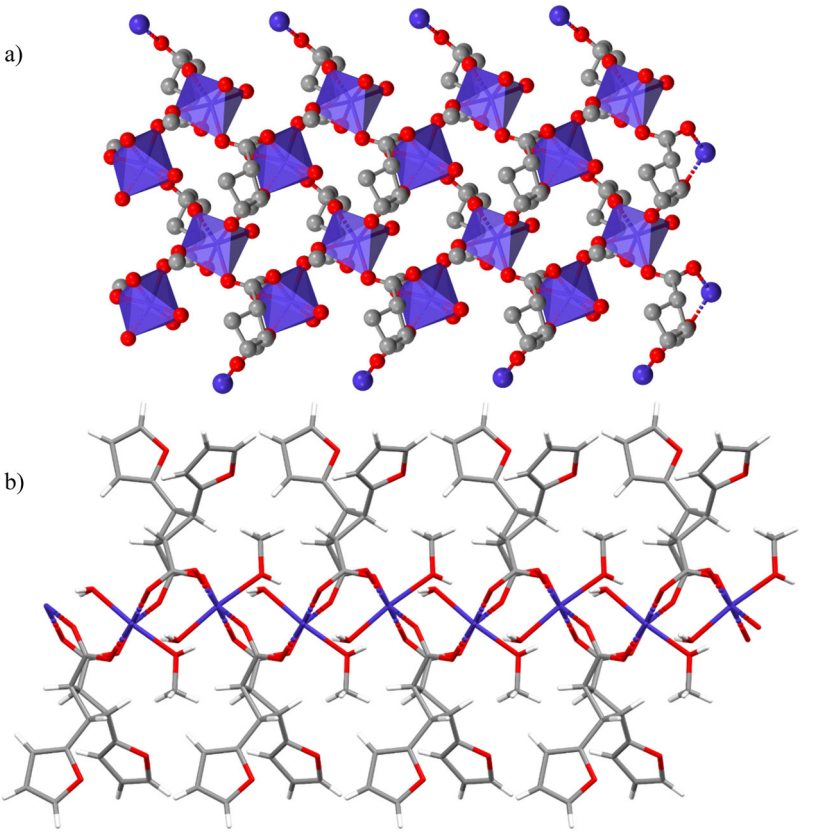

Figure 7. (a) Top view of Co-CBDA-2 (**2**) shown in polyhedral style (the furan substituents are omitted for clarity); (b) Side view of the 2D complex (**2**) along crystallographic *a* axis shown in Capped Sticks style.

The Cu^{2+} interacts with CBDA-2 as illustrated in Figure 3(f), forming a 2D coordination polymer. Figure 5(a) shows a top view of one layer of the 2D structure with the furan substituents omitted for clarity. The Cu^{2+} center is highlighted in polyhedral style. Figure 5(b) shows the side view of the 2D coordination polymer along the crystallographic *a* axis. In the 2D structure, Cu^{2+} cations are sandwiched between two layers of CBDA-2 molecules with the furan substituents pointing outward [32–34]. The oxygen in the furan ring does not participate in interactions with the Cu^{2+} cation or any hydrogen bond. However, the oxygen in the carbonyl group of the deprotonated acid forms two hydrogen bonds (see ESI): one with the hydrogen in the acid of a neighboring CBDA-2 molecule [O···OH distance: 2.601(6) Å] and the other with the hydrogen atom in the hydroxyl group of a MeOH molecule [O···OH distance: 2.604(5) Å].

3.3. Structure description of Co-CBDA-2 (2)

Single-crystal X-ray diffraction analysis revealed that the ratio of Co:CBDA-2:MeOH:H_2O in **2** is 1:1:1:1. Figure 6(a) exhibits the asymmetric unit of **2** in Oak Ridge Thermal Ellipsoid Plot (ORTEP). As shown in Figure 6(b), the Co^{2+} center adopts a slightly

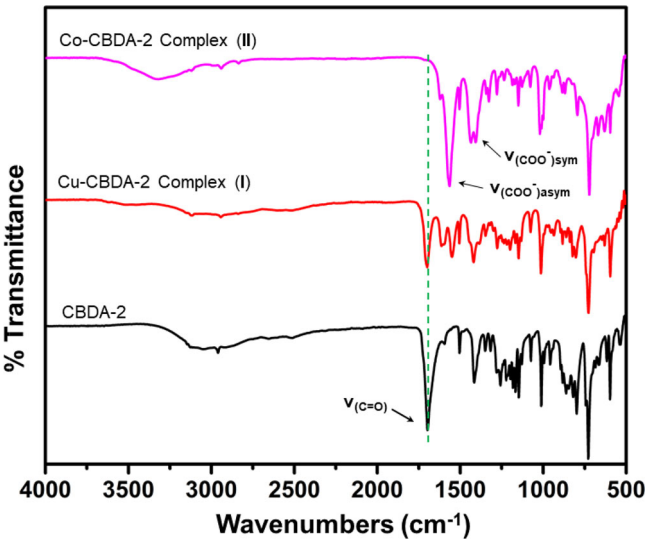

Figure 8. FT-IR spectra of CBDA-2, Cu-CBDA-2 (**1**), and Co-CBDA-2 (**2**).

distorted octahedral geometry with three CBDA-2 molecules interacting with the metal cation in the equatorial basal plane while one MeOH and one H_2O molecule occupy the two opposite axial positions. The O-Co^{2+}-O angle of MeOH, Co^{2+}, and H_2O is 172.4(1)°, and the O-Co^{2+} distances are 2.163(4) and 2.132(4) Å, respectively. Both of the carboxylic acid groups in each CBDA-2 molecule are deprotonated, and they are bonded to the same Co^{2+} cation balancing the charges. The O^{-}-Co^{2+}-O^{-} angle is 95.1(1)°, and the two O^{-}-Co^{2+} bond distances are 2.051(4) and 2.112(3) Å, respectively. Two carbonyl groups from two neighboring CBDA-2 carboxylates occupy the other two corners of the equatorial basal plane of the octahedron, and the two corresponding O-Co^{2+} distances are nearly identical, 2.077(3) and 2.077(4) Å.

The Co^{2+} cation interacts with CBDA-2 as illustrated in Figure 3(h), which is completely different from that (Figure 3f) of Cu-CBDA-2 (**1**). Nevertheless, **2** is also a 2D coordination polymer. Figure 7(a) presents a top view of one layer of the 2D structure with the furan substituents omitted for clarity. The Co^{2+} ion is highlighted in polyhedral style. Figure 7(b) displays the side view of the 2D coordination polymer along the crystallographic *a* axis. Just as in **1**, the Co^{2+} cations are sandwiched between two layers of CBDA-2 molecules with the furan substituents pointing outside. The oxygen in the furan ring does not participate in the interactions with the Co^{2+} cation or any hydrogen bond. However, the MeOH molecule in **2** forms a hydrogen bond with a carboxylate group of a neighboring CBDA-2 ion with O···OH distance of 2.792(5) Å (see ESI). The H_2O in **2** forms two hydrogen bonds with two different carboxylate groups from its two neighboring CBDA-2 ions with O···OH distances of 2.655(5) and 2.991(5) Å (see ESI).

3.4. FT-IR spectra of 1 and 2

The FT-IR spectra of CBDA-2, Cu-CBDA-2 (**1**), and Co-CBDA-2 (**2**) are reported in Figure 8 for comparison. As expected, the strong band at 1698 cm^{-1} in the spectrum of **1**

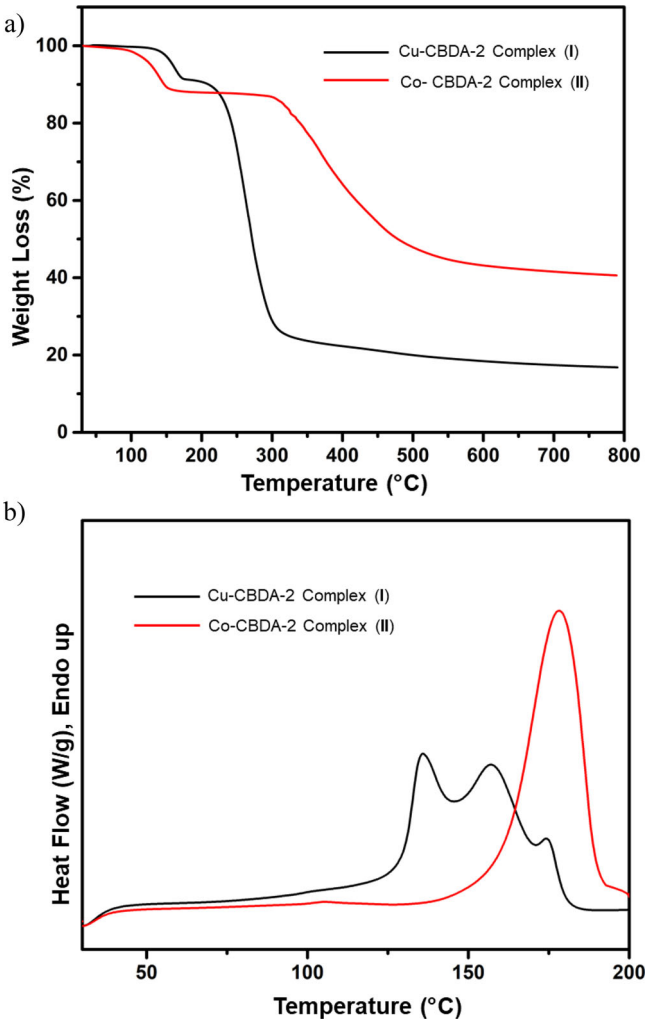

Figure 9. (a) TGA curves of Cu-CBDA-2 (**1**) and Co-CBDA-2 (**2**) with a heating rate of 20 °C min^{-1} under N_2 atmosphere. (b) DSC curves of the two complexes from 25 to 200 °C with a heating rate of 20 °C min^{-1} under N_2.

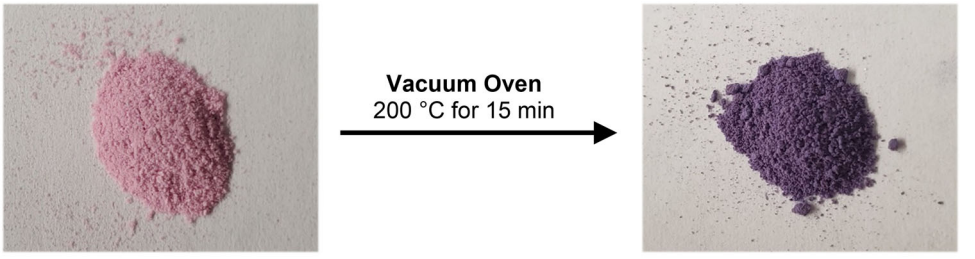

Figure 10. Thermochromic behavior of **2**: (left) sample at room temperature; (right) sample after heated at 200 °C under vacuum for 15 min.

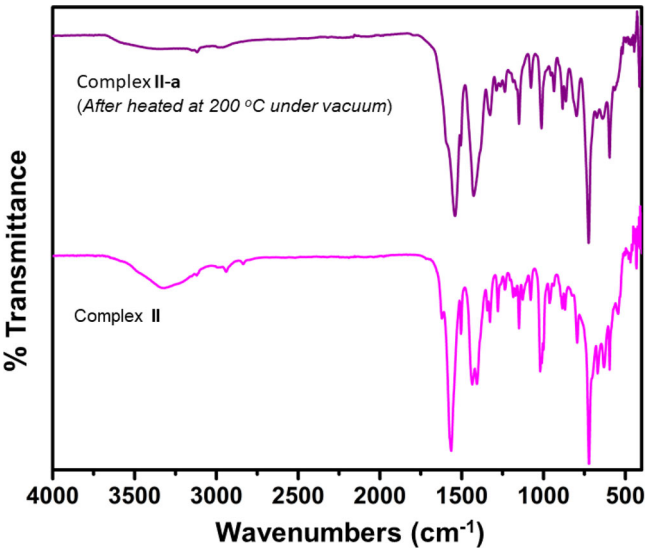

Figure 11. Comparison of the FT-IR spectra of **2** before and after the thermal treatment.

is characteristic of the carbonyl stretching of a carboxylic acid because only one of the two acid groups in CBDA-2 ligand is deprotonated in the complex. In contrast, the peaks at 1564 and 1453 cm^{-1} in the spectrum of **2** are attributed to symmetric and asymmetric stretching of the carboxylate, respectively, since both carboxylic acid groups of CBDA-2 are deprotonated in the complex. Meanwhile, the broad absorption at 3200–3500 cm^{-1} indicates the presence of coordinated H_2O and MeOH molecules in **2**, which is consistent with its single-crystal X-ray structure. For the spectrum of **1**, the hydroxyl stretch of the carboxylic acid is shown beside a weak, broad peak of the hydroxyl stretch of the coordinated MeOH molecules in **1**. At room temperature, the microcrystalline powder of **1** is turquoise while **2** is pink (see ESI for the images of the powder and single crystal samples). The single crystals of the two complexes exhibited the same colors, respectively, but they appeared somewhat lighter.

3.5. Thermal properties of 1 and 2

The thermogravimetric analysis (TGA) and differential scanning calorimetry (DSC) curves of Cu-CBDA-2 complex (**1**) and Co-CBDA-2 complex (**2**) under a nitrogen atmosphere at a heating rate of 20 °C/min are shown in Figure 9, and the corresponding DTG curves are included in the ESI. For comparison, the thermal decomposition profile of CBDA-2 reported in our previous study indicated no degradation below 200 °C. According to the TGA curves in Figure 9(a), both complexes decompose in two stages. Complex **1** exhibited a weight loss of 9.1% due to removal of the coordinated MeOH (calcd.: 9.4%) in the crystalline sample around 150 °C and started to decompose at 200 °C. The TGA curve of **2** showed a weight loss of 12.5%, which accounts for the loss of coordinated MeOH and H_2O molecules at 140 °C (calcd.: 13.1%), but did not decompose until near 300 °C. The latter observations are in accord with the endothermic transitions seen in the DSC curve shown in Figure 9(b). Interestingly, the DSC

curve of **1** displays three overlapped peaks between 120 and 180 °C, indicating possible phase transitions due to the loss of MeOH in the complex. Thermal analysis results indicated a similar thermal decomposition behavior of both complexes, among which **1** decomposes at a lower temperature than **2**, presumably due to the different ways CBDA-2 coordinates to the two metals (i.e. Figure 3f vs. 3h). In short, the two-step decomposition pattern of these 2D coordination polymers is consistent with the SCXRD structural results in terms of ligand coordination to the metal centers.

3.6. Thermochromic properties

Both **1** and **2** showed visual thermochromic behaviors during the study of their thermal properties. When heated to 200 °C for 15 min in a vacuum oven, **1** and **2** turned black and purple, respectively (see Figure 10 and Figure S5 in the ESI). Complex **2** was chosen for further investigation considering its desolvated form showed higher thermal stability and exhibited more interesting color change. In addition, cobalt complexes are present in nature and are included in many synthetic materials with varied applications [35–38]. For example, cobalt is the principle metal of four vitamers of B_{12}, which are deeply red-colored complexes essential to the function of cells.

A comparison of **2** at room temperature and **2-a** after the thermal treatment is shown in Figure 10. The purple color of **2-a** did not change even when the sample was cooled to room temperature and exposed to air. Color changes of metal complexes resulting from temperature variation are mainly caused by solid-solid phase transition due to changes in metal coordination geometry, coordination number, and/or the coordinated ligands [39–43]. The FT-IR spectrum of **2-a** qualitatively indicates that this thermochromic process is likely due to the loss of coordinated MeOH and H_2O molecules, which might have caused the Co^{2+} center to undergo coordination geometry change (Figure 11). The TGA curve of **2** in Figure 9(a) also confirmed that most of the coordinated MeOH and H_2O molecules were removed at 200 °C.

Visual thermochromic materials have found applications in designing security markers in currency bills and bonds [44], smart coatings [45], thermal printing [46], and other merchandise [47]. The successful synthesis and characterization of visual thermochromic complexes **1** and **2**, whose ligand was synthesized from bioadvantaged starting materials, may stimulate more research and development to turn this important and useful area more environmentally friendly [48].

4. Conclusion

A promising biomass-derived ligand, CBDA-2, was introduced to coordination chemistry for the first time in this study. This polytopic ligand was obtained from furfural and malonic acid, which are two bioadvantaged chemicals. A scalable and straightforward synthetic method of CBDA-2 was documented, and single-crystal X-ray data of a mono-carboxylate triethylammonium of CBDA-2 was reported for comparison with other crystal structures. The potential application of CBDA-2 in preparing green metal-organic materials (GMOM) has been demonstrated through the synthesis of two 2D

coordination polymers via a conventional solution method using $Cu(NO_3)_2$ and $Co(NO_3)_2$ as metal sources, respectively. The two 2D complexes have been characterized using single-crystal X-ray diffraction analysis, FT-IR, and TGA/DSC. Although both Cu^{2+} and Co^{2+} in the two 2D structures adopt octahedral geometry while interacting with CBDA-2 and two solvent molecules, this ligand coordinates with the metal cations in two different ways demonstrating its flexibility and adaptability. Moreover, both complexes exhibited visual thermochromic behaviors when heated at 200 °C under vacuum. This oxygen-rich ligand, CBDA-2, and its congeners will provide opportunities to make various green metal-organic materials [11, 49] electronic and optoelectronic devices [50], and functional nanostructured materials with interesting properties and potential applications in the future [51, 52].

Disclosure statement

The authors declare no conflicts of interest.

Funding

This material is based upon work supported by the National Science Foundation Grants (EPSCoR Award IIA-1355466, Grant CHE 1709160, and US MASTER Scholarship Program of S-STEM Award 1742269).

Supporting information

The Supporting Information is available free of charge online: More images of the crystal structures, photos of the crystal and powder samples, FT-IR spectra, DTG curves (PDF) as well as crystal data (CIF).

References

[1] T.A. Bender, J.A. Dabrowski, M.R. Gagné. *Nat. Rev. Chem.*, **2**, 35 (2018).
[2] L.T. Mika, E. Cséfalvay, Á. Németh. *Chem. Rev.*, **118**, 505 (2018).
[3] G. Xu, B. Li, H. Wu, W. Zhou, B. Chen. *Cryst. Growth Des.*, **17**, 4795 (2017).
[4] X.-Y. Wan, F.-L. Jiang, L. Chen, J. Pan, K. Zhou, K.-Z. Su, J.-D. Pang, G.-X. Lyu, M.-C. Hong. *CrystEngComm*, **17**, 3829 (2015).
[5] P. Díaz-Gallifa, O. Fabelo, J. Pasán, L. Cañadillas-Delgado, M.A. Ramírez, A.G. Gallardo, C. Ruiz-Pérez. *CrystEngComm*, **17**, 5081 (2015).
[6] E.M.L. Lippitt, C. Ennis, S.C. Moratti, L.R. Hanton. *Cryst. Growth Des.*, **20**, 7805 (2020).
[7] L.R. MacGillivray, G.S. Papaefstathiou, T. Friscić, T.D. Hamilton, D.-K. Bucar, Q. Chu, D.B. Varshney, I.G. Georgiev. *Acc. Chem. Res.*, **41**, 280 (2008).
[8] L.N. Dawe, K.V. Shuvaev, L.K. Thompson. *Chem. Soc. Rev.*, **38**, 2334 (2009).
[9] S. Zhan, J.A. De Gracia Triviño, M.S.G. Ahlquist. *J. Am. Chem. Soc.*, **141**, 10247 (2019).
[10] X. Zhang, B. Li, Z.-H. Chen, Z.-N. Chen. *J. Mater. Chem.*, **22**, 11427 (2012).
[11] S. Kumar, S. Jain, M. Nehra, N. Dilbaghi, G. Marrazza, K.-H. Kim. *Coord. Chem. Rev.*, **420**, 213407 (2020).
[12] J. Chen, K. Shen, Y. Li. *ChemSusChem*, **10**, 3165 (2017).
[13] Z. Wang, M. Scheuring, M. Mabin, R. Shahni, Z.D. Wang, A. Ugrinov, J. Butz, Q.R. Chu. *ACS Sustainable Chem. Eng.*, **8**, 8909 (2020).
[14] Z.D. Wang, Q. Elliott, Z. Wang, R.A. Setien, J. Puttkammer, A. Ugrinov, J. Lee, D.C. Webster, Q.R. Chu. *ACS Sustainable Chem. Eng.*, **6**, 8136 (2018).

[15] Z. Wang, B. Kastern, K. Randazzo, A. Ugrinov, J. Butz, D.W. Seals, M.P. Sibi, Q.R. Chu. *Green Chem.*, **17**, 4720 (2015).
[16] R. Mariscal, P. Maireles-Torres, M. Ojeda, I. Sádaba, M.L. Granados. *Energy Environ. Sci.*, **9**, 1144 (2016).
[17] X. Li, P. Jia, T. Wang. *ACS Catal.*, **6**, 7621 (2016).
[18] https://repository.upenn.edu/cgi/viewcontent.cgi?article=1100&context=cbe_sdr (accessed Dec. 10, 2020).
[19] https://lygos.com/app/uploads/2015/03/2014-12-Website-Flyer.pdf (accessed Dec. 10, 2020).
[20] R. Wang, Y. Zhou, Y. Sun, D. Yuan, L. Han, B. Lou, B. Wu, M. Hong. *Cryst. Growth Des.*, **5**, 251 (2005).
[21] D. Avcı, S. Altürk, F. Sönmez, Ö. Tamer, A. Başoğlu, Y. Atalay, B. Zengin Kurt, D. Öztürk, N. Dege. *Appl. Organometal. Chem.*, **33**, e4725 (2019).
[22] D. Ma, P. Hu, L. Qin, J. Yan, W. Lin, W. Ding, H. Lu, D. Lin, H. Sakiyama, F. Liang. *J. Inorg. Organomet. Polym.*, **26**, 1053 (2016).
[23] E. Lagerspets, K. Lagerblom, E. Heliövaara, O.-M. Hiltunen, K. Moslova, M. Nieger, T. Repo. *Mol. Catal.*, **468**, 75 (2019).
[24] D. Shi, C.-J. Cui, M. Hu, A.H. Ren, L.-B. Song, C.-S. Liu, M. Du. *J. Mater. Chem. C*, **7**, 10211 (2019).
[25] P. Thuéry, Y. Atoini, J. Harrowfield. *Inorg. Chem.*, **59**, 6953 (2020).
[26] Q.L. Guan, X. Gao, J. Liu, W.J. Wei, Y.H. Xing, F.Y. Bai. *J. Coord. Chem.*, **69**, 1026 (2016).
[27] L.A. Essex, A. McSkimming, N.B. Thompson, M.L. Kelty, E.A. Hill, W.H. Harman. *Organometallics*, **39**, 2545 (2020).
[28] F.A. Cotton, B.A. Frenz. *Tetrahedron*, **30**, 1587 (1974).
[29] Z. Wang, B. Miller, M. Mabin, R. Shahni, Z.D. Wang, A. Ugrinov. *Q.R. Chu. Sci. Rep.*, **7**, 13704 (2017).
[30] H. Amjaour, Z. Wang, M. Mabin, J. Puttkammer, S. Busch, Q.R. Chu. *Chem. Commun. (Camb.)*, **55**, 214 (2019).
[31] R.K. Shahni, M. Mabin, Z. Wang, M. Shaik, A. Ugrinov, Q.R. Chu. *Polym. Chem.*, **11**, 6081 (2020).
[32] X. Hou, Z. Wang, M. Overby, A. Ugrinov, C. Oian, R. Singh, Q.R. Chu. *Chem. Commun. (Camb.)*, **50**, 5209 (2014).
[33] Z. Wang, J. Lee, C. Oian, X. Hou, Z. Wang, A. Ugrinov, R.K. Singh, E. Wysocki, Q.R. Chu. *CrystEngComm*, **16**, 7176 (2014).
[34] X. Hou, M. Schober, Q. Chu. *Cryst. Growth Des.*, **12**, 5159 (2012).
[35] A. Mishra, A. Ali, S. Upreti, M.S. Whittingham, R. Gupta. *Inorg. Chem.*, **48**, 5234 (2009).
[36] X.-D. Yang, R. Zhu, J.-P. Yin, L. Sun, R.-Y. Guo, J. Zhang. *J. Zhang. Cryst. Growth Des.*, **18**, 3236 (2018).
[37] A.K. Renfrew, E.S. O'Neill, T.W. Hambley, E.J. New. *Coord. Chem. Rev.*, **375**, 221 (2018).
[38] X. Xie, C. He, B. Li, Y. He, D.A. Cullen, E.C. Wegener, A.J. Kropf, U. Martinez, Y. Cheng, M.H. Engelhard, M.E. Bowden, M. Song, T. Lemmon, X.S. Li, Z. Nie, J. Liu, D.J. Myers, P. Zelenay, G. Wang, G. Wu, V. Ramani, Y. Shao. *Nat. Catal.*, **3**, 1044 (2020).
[39] C.-L. Chen, A.M. Goforth, M.D. Smith, C.-Y. Su, H.-C. Zur Loye. *Angew. Chem. Int. Ed. Engl.*, **44**, 6673 (2005).
[40] K. Takaoka, M. Kawano, M. Tominaga, M. Fujita. *Angew. Chem. Int. Ed. Engl.*, **44**, 2151 (2005).
[41] S.-J. Fu, C.-Y. Cheng, K.-J. Lin. *Cryst. Growth Des.*, **7**, 1381 (2007).
[42] T. Lasanta, M.E. Olmos, A. Laguna, J.M. López-de-Luzuriaga, P. Naumov. *J. Am. Chem. Soc.*, **133**, 16358 (2011).
[43] C. Shen, T. Sheng, Q. Zhu, S. Hu, X. Wu. *CrystEngComm*, **14**, 3189 (2012).
[44] G. Payne. *Chem. Br.*, **38**, 37 (2002).
[45] J. Nicholls. *Mater. World*, **4**, 19 (1996).
[46] G.K. Sacripante. *Chem. Br.*, **37**, 52 (2001).
[47] G.D. White, D.A. Zartman, J.M. Bonicamp. *Chem. Educator*, **5**, 2 (2000).

[48] I.T. Horváth. *Chem. Rev.*, **118**, 369 (2018).
[49] Q. Chu, A.J.E. Duncan, G.S. Papaefstathiou, T.D. Hamilton, M.B.J. Atkinson, S.V.S. Mariappan, L.R. MacGillivray. *J. Am. Chem. Soc.*, **140**, 4940 (2018).
[50] V. Stavila, A.A. Talin, M.D. Allendorf. *Chem. Soc. Rev.*, **43**, 5994 (2014).
[51] J. Chen, X. Wu, X. Hou, X. Su, Q. Chu, N. Fahruddin, J.X. Zhao. *ACS Appl. Mater. Interfaces*, **6**, 21921 (2014).
[52] K.J. Lee, J.H. Lee, S. Jeoung, H.R. Moon. *Acc. Chem. Res.*, **50**, 2684 (2017).